Evaluation of the Effect of Glucose Ingestion and Kinetic Model Configurations of FDG in the Normal Liver

Yong Choi, Randall A. Hawkins, Sung-Cheng Huang, Richard C. Brunken, Carl K. Hoh, Cristina Messa, Egbert U. Nitzsche, Michael E. Phelps and Heinrich R. Schelbert

Division of Nuclear Medicine and Biophysics, Department of Molecular and Medical Pharmacology, Laboratory of Nuclear Medicine (DOE), Laboratory of Structural Biology and Molecular Medicine and The Crump Institute for Biological Imaging, School of Medicine, University of California, Los Angeles, California

The liver plays an important role in glucose homeostasis. PET studies with 2-[F-18]fluoro-2-deoxy-D-glucose (FDG) of the liver (e.g., in neoplasms) require an understanding of the effects of dietary conditions on hepatic FDG uptake. **Methods:** Twenty studies were performed on 10 normal volunteers (ages 24 ± 4) after fasting 4 to 19 hr and again after oral consumption of 100 g of dextrose to investigate tracer kinetic model configurations of FDG in the normal liver and to evaluate the impact of oral glucose on liver in normal subjects. Dynamic PET images were acquired for about 1 hr using a Siemens/CTI 931 tomograph. **Results:** A three-compartment model with an input function delay time parameter was the statistically preferred model configuration. The model estimated transport rate constant from plasma to liver, K_1, increased significantly ($p < 0.05$) from 0.864 ± 0.136 ml/min/g in fasting studies to 1.058 ± 0.269 ml/min/g in postglucose studies. Glucose loading also significantly increased ($p < 0.01$) the rate constant for FDG phosphorylation, k_3, from 0.005 ± 0.003 min^{-1} in fasting studies to 0.013 ± 0.007 min^{-1} in postglucose administration and, consequently, significantly increased both the phosphorylation fraction ($k_3/(k_2 + k_3)$) and the influx constant ($K_1k_3/(k_2 + k_3)$). No significant differences in the liver-to-plasma transport rate constant, k_2, dephosphorylation constant, k_4, or distribution volume of FDG ($K_1/(k_2 + k_3)$) were observed. **Conclusion:** Dynamic FDG-PET studies can be used to evaluate kinetics of liver glucose metabolism. The results indicate that dietary conditions have a significant effect on hepatic FDG kinetics. Because of the higher net FDG uptake by normal liver after glucose loading, fasting conditions are preferred for FDG liver tumor studies to increase the tumor-to-background contrast.

Key Words: liver glucose metabolic rates; effect of oral glucose; fluorodeoxy-D-glucose; positron emission tomography

J Nucl Med 1994; 35:818–823

Received Aug. 25, 1993; revision accepted Jan. 20, 1994.

For correspondence or reprints contact: Yong Choi, PhD, PET Facility, B-938, Department of Radiology, University of Pittsburgh Medical Center, 200 Lothrop Street, Pittsburgh, PA 15213-2582.

The liver is an important component in the regulation of plasma glucose concentrations. After carbohydrate intake, increasing glucose concentrations in the plasma inactivates glycogen phosphorylase$_a$ and activates glycogen synthetase. This leads to hepatic glycogen synthesis. These direct actions of glucose stimulating the synthesis and storage of glycogen are reinforced by increased secretion of insulin. During fasting, the reaction steps are reversed and stored glycogen is metabolized. The blood glucose level is, therefore, buffered by the liver.

PET with 2-[F-18]fluoro-2-deoxy-D-glucose (FDG) has been demonstrated to be useful in the evaluation of malignant tumors and other liver diseases (*1–2*). In order to interpret hepatic FDG studies meaningfully, however, one must understand normal hepatic FDG kinetics and the effect of dietary influences on these studies.

The purposes of this study are:

1. To investigate different tracer kinetic model configurations of FDG (including two-compartment model, three-compartment model, three-compartment model with vascular volume parameter, and three-compartment model with input function time delay parameter) in the liver.
2. To determine the optimal tracer kinetic model.
3. To use the best model configuration to evaluate the impact of oral glucose loading on liver in normal subjects.

MATERIALS AND METHODS

Human Subjects

Ten healthy male volunteers (age: 24 ± 4 years, range: 18 to 31 years) were studied after they gave written, informed consent. The experimental protocol was approved by the UCLA Human Subject Protection Committee. Each subject was studied after fasting 9 ± 4 hr (ranging 4–16 hr) and again 1 hr after orally consuming 100 g of dextrose in aqueous solution (Tru-Glu™, Fisher Scientific, Pittsburgh, PA). PET studies included in this investigation have been reported, in part, in another study (*3*); this work, however, addresses an entirely different issue.

PET Imaging

Sterile FDG (*4,5*) was produced at the UCLA Biomedical Cyclotron Facility. Separate intravenous lines were placed in a dorsal vein of each hand for injection of FDG and for blood sampling respectively. Each subject received a total dose of 10 mCi of FDG. FDG diluted in about 8 ml saline solution was injected intravenously over 30 sec using an infusion pump. The line was then flushed with an additional 10 ml saline solution over the next 30 sec.

Serial image acquisition was begun at the time of the FDG injection and consisted of ten 10-sec, two 40-sec, two 300-sec, and five 600-sec frames for a total imaging time of 63 min. Transaxial images were acquired on a Siemens/CTI 931/08-12 tomograph (Siemens, Hoffman Estates, IL) which simultaneously records 15 contiguous planes. Each subject was positioned to allow image acquisition of the left ventricular cavity and superior aspect of the liver in a supine position. The interplane spacing was 6.75 mm and encompassed a 108-mm axial field of view.

The 15 contiguous transaxial dynamic images were reconstructed employing a Shepp-Logan filter with a cutoff at 0.3 Nyquist frequency, resulting in an effective in-plane resolution of about 10 mm FWHM. The scanner's axial resolution was approximately 7 mm FWHM. Emission images were corrected for photon attenuation using a 20-min transmission scan obtained from a $^{68}Ge/^{68}Ga$ external ring source.

Blood Sampling

Four arterialized venous blood samples were obtained from a dorsal hand vein heated to 43°C to arterialize the venous blood at 30, 40, 50 and 60 min after FDG injection (*6*). These blood samples were immediately centrifuged to separate plasma. Plasma ^{18}F concentrations were assayed and these concentrations were used to correct for spillover of activity from the left ventricular myocardium to the blood pool using a previously reported technique (*7*).

A cylindrical phantom, 20 cm in diameter containing $^{68}Ge/^{68}Ga$, was imaged before each study. An aliquot of the $^{68}Ge/^{68}Ga$ solution in the cylinder was placed in a well counter in order to obtain a conversion factor that related image data (counts/pixel/second) to well counter data (counts/ml/sec).

Plasma glucose concentrations (C_p) were measured at about 0, 30 and 60 min following the administration of FDG. Arterial plasma or serum concentrations of insulin, glucagon and lactate were measured during each study approximately 30 min after FDG injection.

Image Analysis

Regional liver tissue time-activity curves were generated from region of interests (ROIs), with an area of about 50 cm^2, constructed over the right lobe of the liver (Fig. 1). The arterial input function was derived from a ROI, about 0.6 cm^2 in size, assigned to the left ventricular cavity on the dynamic PET images (Fig. 1) (*8,9*). Spillover of activity from myocardium into the left ventricular cavity (SP_{TC}) was corrected using in vitro measurements of plasma samples obtained from a heated hand vein (*7*). These corrected input functions eliminate the bolus delay and dispersion effects inherent in input functions acquired from a peripheral site, and SP_{TC} effects confounding input functions derived from the dynamic PET images.

Mathematical Model

A three-compartment model for FDG, originally developed for the brain (*6,10,11*) and applied to the heart (*7,9,12*) and tumors (*1,13*), was utilized for evaluation of FDG kinetics in liver. Additionally, the following different model configurations were evaluated to choose an optimal tracer kinetic model for the liver FDG studies: (1) two-compartment model consisting of FDG in plasma and FDG-6-phosphate in tissue; (2) three-compartment model consisting of FDG in plasma, FDG in tissue and FDG-6-phosphate in tissue; (3) three-compartment model with vascular volume parameter (V); and (4) three-compartment model with input function time delay parameter (TD).

The solution equations, $C_t(t)$, for the model configurations 1–4 using the time-activity curve for the left ventricular cavity as an input function, $C_p(t)$, are as follows:

Configuration 1

$$C_t(t) = K_1 e^{-k_2 t} \otimes C_p(t) \qquad \text{Eq. 1}$$

Configuration 2

$$C_t(t) = \frac{K_1}{\alpha_2 - \alpha_1}[(k_3 + k_4 - \alpha_1)e^{-\alpha_1 t} + (\alpha_2 - k_3 - k_4)e^{-\alpha_2 t}] \otimes C_p(t) \qquad \text{Eq. 2}$$

Configuration 3

$$C_t(t) = \frac{K_1}{\alpha_2 - \alpha_1}[(k_3 + k_4 - \alpha_1)e^{-\alpha_1 t} + (\alpha_2 - k_3 - k_4)e^{-\alpha_2 t}] \otimes C_p(t) + VC_p(t) \qquad \text{Eq. 3}$$

Configuration 4

$$C_t(t) = \frac{K_1}{\alpha_2 - \alpha_1}[(k_3 + k_4 - \alpha_1)e^{-\alpha_1 t} + (\alpha_2 - k_3 - k_4)e^{-\alpha_2 t}] \otimes C_p(t + TD), \qquad \text{Eq. 4}$$

where

$$\alpha_{2,1} = [(k_2 + k_3 + k_4) \pm \sqrt{(k_2 + k_3 + k_4)^2 - 4k_2k_4}]/2.$$

The rate constant K_1 refers to blood flow because it represents both the tracer delivery to the cells by blood flow and the extraction of the tracer across the capillary tissue interface, and because the littoral cells, the endothelial cells of the sinusoids of the liver, allow an almost free exchange even of macromolecules between blood and the narrow perisinusoidal spaces (*14*). The reverse transport rate constants are k_2 (min^{-1}) and k_2' (min^{-1}) in the three- and two-compartment models respectively. The rate constants k_3 (min^{-1}) and k_4 (min^{-1}) in the three-compartment model refer to the phosphorylation of FDG and dephosphorylation of FDG-6-phosphate respectively.

Model configuration 3 includes a vascular volume parameter, V, to account for nonextracted FDG activity remaining within the liver tissue vascular space. The input function time delay parameter (TD) is included in model configuration 4 to account for the time difference between the time-activity curve in the left ventricular cavity and that of the input to the liver, which consists of hepatic arterial and portal vein supplies.

The nonlinear least squares fit was applied to kinetic data which are proportionately weighted to frame duration to estimate each rate constant. Phosphorylation fraction (PF), distribution volume (DV) and influx constant (K) for the three-compartment model are given by the following equations:

$$PF = \frac{k_3}{(k_2 + k_3)} \quad \text{Eq. 5}$$

$$DV\ (ml/g) = \frac{K_1}{(k_2 + k_3)} \quad \text{Eq. 6}$$

$$K\ (ml/min/g) = \frac{K_1 k_3}{(k_2 + k_3)} \quad \text{Eq. 7}$$

Statistical Analysis

Statistical comparisons were performed to identify the most efficient model configuration, defined as the model with the fewest number of parameters that accurately fit the data (*15,16*). Because regression routines involve minimizing the residual sum of squares (RSS), adding a parameter to a model often decreases the RSS even if the fit is not significantly better. As recommended by Landaw and DiStefano (*16*), three methods can be employed to identify a statistically favorable model: the F statistic, the Akaike information criterion (*17*) and the Schwartz criterion (*18*).

The F statistic is computed by the following equation:

$$F = \frac{(RSS_1 - RSS_2)/P_2 - P_1)}{RSS_2/(N - P_2)}, \quad \text{Eq. 8}$$

where RSS_1 and RSS_2 refer to the residual sum of squares for the lower- and higher-order models respectively, P_1 and P_2 are the number of parameters in the alternative configurations and N is the total number of data points (19 in this study). The F statistic has $(P_2 - P_1, N - P_2)$ degrees of freedom. Probability (p) value less than an acceptable limit (e.g. 0.05) rejects the null hypothesis that the parameter model with the fewer parameters is preferred.

The Akaike information criterion (AIC) and the Schwarz criterion (SC) are defined by:

$$AIC = N \ln(RSS) + 2P \quad \text{Eq. 9}$$

and

$$SC = N \ln(RSS) + P \ln(N) \quad \text{Eq. 10}$$

respectively, where P is the number of parameters of a model configuration. The Akaike information criterion and Schwarz criterion generate a numerical score of the adequacy of the model using Equations 9 and 10. The model configuration with the lowest score is preferred.

Pairwise comparisons were performed using paired t-tests with the Bonferroni correction. The significance of the correlation coefficients, r, was determined using nondirectional (two-tailed) tests; p values less than 0.05 were considered statistically significant.

RESULTS

Hemodynamics, Substrate and Hormone Concentrations

Although the average heart rate increased after oral glucose, the average systolic blood pressures and rate-pressure products did not differ significantly between fasting and postglucose studies (Table 1). Glucose loading increased plasma glucose and insulin levels and decreased glucagon levels in each individual. Lactate levels were similar for fasting and postglucose studies.

TABLE 1
Hemodynamics, Substrate and Hormone Concentrations and Model Parameters

	Fasting	Postglucose	
Heart rate (min^{-1})*	64 ± 6	70 ± 9	$p < 0.05$
SBP (mmHg)	113 ± 11	113 ± 8	ns
RPP (mmHg/min)*	7242 ± 1106	8059 ± 1500	ns
Glucose (mg/dl)	89 ± 5	158 ± 34	$p < 0.001$
Lactate (mg/dl)*	6.2 ± 1.5	7.2 ± 1.2	ns
Insulin (mcU/ml)	8 ± 4	43 ± 20	$p < 0.001$
Glucagon (pg/ml)	99 ± 41	59 ± 23	$p < 0.001$

Values represent averages ± s.d. in 10(9*) paired fasting and postglucose studies.
SBP = systolic blood pressure; RPP = rate-pressure product.

Time-Activity Distribution of FDG in Liver

Vascular activities were prominent early after tracer injection on images of both the midventricular myocardium and the liver (Fig. 1). At 60 min after FDG injection, ^{18}F radioactivity had accumulated in the myocardium while it decreased slowly from liver (Fig. 1). Typical time-activity curves of liver and input functions are illustrated in Figure 2. For both the fasting and postglucose studies, liver activity cleared concordantly with blood FDG activity. However, FDG accumulation in liver compared to blood FDG was more obvious in the postglucose studies.

Comparisons of Model Configurations

The data did not fit a simple two-compartment model well. All three statistical methods revealed that the three-compartment model was superior to the two-compartment model (Table 2). On the basis of the three statistical methods, the five-parameter three-compartment model, including vascular volume or input function time delay parameter, was superior to the four-parameter three-compartment

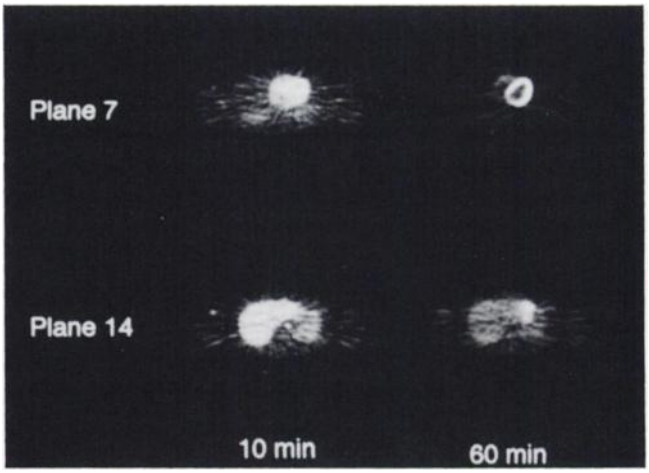

FIGURE 1. Two different transaxial images over the midventricular area of the heart and over the liver obtained 10 and 60 min after the FDG injection. The shape of arterial input function was derived from the left ventricular blood pool, and liver tissue time-activity curves were derived from right lobe of the liver.

TABLE 2
Comparisons of Model Configurations

F statistic				
No. of parameters	Two 2	Three 4	Three + V 5	Three + TD 5
Two	—	*	*	*
Three	$p < 0.01$	—	*	*
Three + V	$p < 0.001$	$p < 0.001$	—	†
Three + TD	$p < 0.001$	$p < 0.001$	†	—

Akaike information criterion			
Two	Three	Three + V	Three + TD
56.7	47.8	34.5	20.6

Schwarz criterion			
Two	Three	Three + V	Three + TD
58.6	51.6	39.2	25.4

*The null hypothesis is that the lower-order model is correct compared to the higher-order model.

†The F statistics cannot be computed for the model configurations having the same number of parameters.

Two = two-compartment model; Three = three-compartment model; three + V = three-compartment model with vascular volume parameter; Three + TD = three-compartment model with input function time delay parameter.

model (Table 2). Of the five-parameter model configurations, the Akaike information criterion and the Schwartz criterion can be used to score the models and to identify the statistically favorable model. Based on the Akaike information criterion and the Schwartz criterion, the five-parameter model with parameters for the input function time delay was superior to the model with the vascular volume parameter (Table 2).

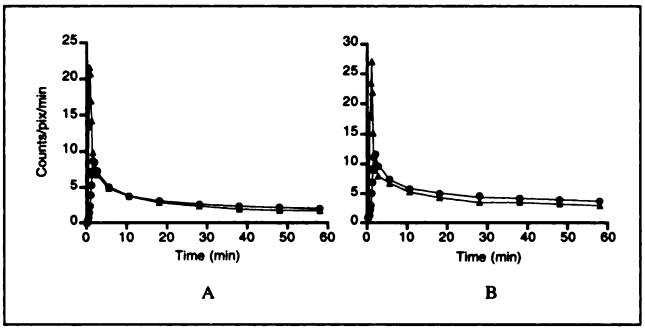

FIGURE 2. Plasma input function (▲) and liver tissue time-activity curves (●) in a fasting study (A) and a postglucose (B) study. The smooth line through the liver tissue kinetic data is the three-compartment model (including input function time delay parameter) fit to the data. A line (linear interpolation) was also drawn through the input function data to illustrate the shape of the curve.

Parameter Estimates

The three-compartment model with input function time delay parameter fits the kinetic data well for both fasting and postglucose studies (Fig. 2). The model parameters of the three-compartment model with input function time delay for fasting and postglucose studies are shown in Table 3. The model estimated transport rate constant, K_1, was 0.864 ± 0.136 and 1.058 ± 0.269 ml/min/g in the fasting and postglucose studies respectively, and significantly ($p < 0.05$) increased after oral glucose (Table 3). Glucose loading significantly ($p < 0.01$) increased the rate constant for FDG phosphorylation from 0.005 ± 0.003 to 0.013 ± 0.007 min^{-1} and, consequently, significantly increased the phosphorylation fraction (Equation 5) and the influx constant (Equation 7). No significant differences in the reverse transport rate constant, k_2, dephosphorylation constant, k_4, input function delay time, TD, or distribution volume of FDG were observed in different dietary states.

DISCUSSION

The choice of model configuration for a given dataset can be determined by biochemical and physiological supporting data and statistical analyses. An effective operational approach is selecting a model with the fewest number of parameters that adequately fit the data, while maintaining a biologically relevant model configuration (*16*). The results from model fitting and statistical analysis indicate that the two-compartment model is insufficient for evaluating the transport and phosphorylation of FDG in the liver and that the conventional three-compartment model employed for brain and heart studies adequately describes the kinetics of FDG in normal liver.

The liver is supplied by dual vascular inputs (hepatic artery and portal vein). In normal subjects, the portal vein supplies about 70% of the hepatic vascular input and the hepatic artery supplies about 30% (*14*). Because FDG extraction in portal circulation should be small and a major portion (>70%) of FDG is delivered via the portal vein, it would be reasonable to assume a single input with a finite time delay. The model estimate of time delay of input was 0.297 ± 0.073 min in fasting and 0.273 ± 0.119 min in postglucose studies. A significant improvement in the model fit to the data was achieved by adding the time delay parameter.

The transport rate constant, K_1, representing liver blood flow was 0.864 ± 0.136 ml/min/g and 1.058 ± 0.269 ml/min/g in fasting and postglucose studies respectively. These values are in close agreement with the previously reported hepatic blood flow value of 1 ml/min/g (*14,19*). The increment in liver blood flow after oral glucose loading observed in this study, 22.5%, is in close agreement with the value of 29.6% observed in rats (*20*).

Glucose loading increased the phosphorylation rate constant, k_3, 2.6-fold in normal subjects. This increment in phosphorylation rate is similar to the results observed in rat liver after fructose administration (*21*). A relatively high

TABLE 3
Three-Compartment Model Parameters with Input Function Time Delay

	K_1 ml/min/g	k_2 min^{-1}	k_3 min^{-1}	k_4 min^{-1}	TD min	PF	DV ml/g	K ml/min/g	Glu mg/dl	K · Glu μmole/min/g
Fasting										
1	0.719	0.788	0.003	0.000	0.245	0.004	0.909	0.003	92	0.014
2	0.889	1.062	0.004	0.000	0.241	0.003	0.834	0.003	97	0.016
3	0.987	0.998	0.006	0.042	0.181	0.005	0.984	0.005	83	0.025
4	0.708	0.817	0.008	0.085	0.352	0.010	0.857	0.007	90	0.035
5	0.845	1.019	0.004	0.000	0.317	0.004	0.826	0.003	81	0.013
6	0.708	0.865	0.004	0.000	0.451	0.004	0.815	0.003	86	0.014
7	1.107	1.274	0.000	0.000	0.288	0.000	0.869	0.000	88	0.000
8	0.786	0.750	0.004	0.000	0.323	0.005	1.042	0.004	97	0.023
9	0.916	1.104	0.011	0.029	0.303	0.010	0.822	0.009	87	0.044
10	0.978	1.134	0.005	0.005	0.273	0.004	0.859	0.004	90	0.021
Avg.	0.864	0.981	0.005	0.016	0.297	0.005	0.882	0.004	89	0.021
s.d.	0.136	0.171	0.003	0.028	0.073	0.003	0.076	0.003	5	0.012
Postglucose										
1	1.063	1.179	0.010	0.007	0.232	0.008	0.894	0.009	194	0.097
2	1.151	1.348	0.007	0.000	0.253	0.005	0.850	0.006	213	0.067
3	1.147	1.444	0.017	0.013	0.233	0.011	0.786	0.013	186	0.136
4	1.345	1.477	0.016	0.034	0.325	0.011	0.901	0.015	155	0.125
5	0.709	0.871	0.014	0.039	0.173	0.016	0.802	0.011	100	0.063
6	0.452	0.589	0.006	0.000	0.577	0.011	0.759	0.005	155	0.042
7	1.161	1.161	0.005	0.002	0.258	0.004	0.996	0.005	174	0.046
8	1.128	1.398	0.023	0.016	0.231	0.016	0.794	0.018	143	0.146
9	1.170	1.024	0.022	0.027	0.303	0.021	1.118	0.025	130	0.180
10	1.251	1.325	0.009	0.000	0.148	0.006	0.938	0.008	130	0.059
Avg.	1.058*	1.182	0.013†	0.014	0.273	0.011†	0.884	0.011*	158†	0.096†
s.d.	0.269	0.284	0.007	0.015	0.119	0.006	0.112	0.007	34	0.048

*$p < 0.05$ compared with the values of fasting studies.
†$p < 0.01$ compared with the values of fasting studies.
TD (min) = input function time delay parameter; PF = phosphorylation fraction; DV (ml/g) = distribution volume of FDG; K (ml/min/g) = influx constant; Glu (mg/dl) = plasma glucose concentration; K · Glu (μmole/min/g) = influx constant times plasma glucose concentration.

value for the dephosphorylation rate constant, k_4, was observed. This is consistent with the high level of glucose-6-phosphatase in the liver. Because of the low signal, however, the k_4 values in normal liver (Table 3) show large standard deviations and a comparison of the magnitude of the dephosphorylation rate in different dietary states is difficult.

Liver glucose metabolic rates (μmole/min/g) can be calculated by multiplying the influx constant, K (ml/min/g), by plasma glucose concentration (μmole/ml) (Table 3). However, differences in the transport and phosphorylation of FDG and glucose, expressed by an empirically derived lumped constant, should be taken into account (*10*). A lumped constant in the liver remains to be determined for the calculation of liver glucose metabolic rates using FDG.

A three-compartment model with an input function time delay parameter fits the liver FDG kinetic data well. The hepatic phosphorylation rate of FDG is significantly increased by glucose loading. The fasting state will be preferred for PET-FDG studies of the liver tumor because glucose loading increases influx of FDG into normal liver while decreasing influx of FDG into liver tumor (*22*), causing decrement of normal to tumor contrast.

ACKNOWLEDGMENTS

The authors thank Denis B. Buxton, PhD, N. Satyamurthy, PhD, Ron Sumida, Larry Pang, Francine Aguilar, and Eileen Rosenfeld for their help in performing this project. This work was supported in part by the Director of the Office of Energy Research, Office of Health and Environmental Research, Washington, DC, and by research grants #HL 29845 and #HL 33177, National Institute of Health, Bethesda, MD.

REFERENCES

1. Messa C, Choi Y, Hoh CK, et al. Quantitative evaluation of glucose utilization in liver metastasis: utility of parametric imaging with PET. *J Comput Assist Tomogr* 1992;16(5):684–689.
2. Eastman RC, Carson RE, Orloff DG, et al. Glucose utilization in a patient with hepatoma and hypoglycemia: assessment by a positron emission tomography. *J Clin Invest* 1992;89:1958–1963.
3. Choi Y, Brunken RC, Hawkins RA, et al. Factors affecting myocardial 2-[F-18]fluoro-2-deoxy-D-glucose uptake in positron emission tomography studies of normal humans. *Eur J Nucl Med* 1993;20:308–318.
4. Ido T, Wan WN, Casella V, et al. Labeled 2-deoxy-D-glucose analogs: ^{18}F-labeled 2-deoxy-2-fluoro-D-glucose, 2-deoxy-2-fluoro-D-mannose, and ^{14}C-2-deoxy-2-fluoro-D-glucose. *J Lab Compd Radiopharm* 1978;14:174–183.
5. Padgett HC, Schmidt DG, Luxen A, Bida GT, Satyamurthy N, Barrio JR. Computer-controlled radiochemical synthesis: a chemistry process control unit for the automated production of radiochemicals. *Appl Radiat Isot* 1989;40:433–445.

6. Phelps ME, Huang SC, Hoffman EJ, Selin CJ, Sokoloff L, Kuhl DE. Tomographic measurement of local cerebral glucose metabolic rate in humans with (F-18)2-fluoro-d-deoxy-D-glucose: validation of method. *Ann Neurol* 1979;6:371–388.
7. Choi Y, Hawkins RA, Huang SC, et al. Parametric images of myocardial metabolic rate of glucose generated from dynamic cardiac PET and 2-[^{18}F]fluoro-2-deoxy-D-glucose studies. *J Nucl Med* 1991;32:733–738.
8. Weinberg IN, Huang SC, Hoffman EJ, et al. Validation of PET-acquired input functions for cardiac studies. *J Nucl Med* 1988;29:241–247.
9. Gambhir SS, Schwaiger M, Huang SC, et al. Simple noninvasive quantification method for measuring myocardial glucose utilization in humans employing positron emission tomography and fluorine-18-deoxyglucose. *J Nucl Med* 1989;30:356–366.
10. Sokoloff L, Reivich M, Kennedy C, et al. The [^{14}C]deoxyglucose method for the measurement of local cerebral glucose utilization: theory, procedure, and normal values in the conscious and anesthetized albino rat. *J Neurochem* 1977;28:897–916.
11. Huang SC, Phelps ME, Hoffman EJ, et al. Noninvasive determination of local cerebral metabolic rate of glucose in man. *Am J Physiol* 1980;238:E69–E82.
12. Phelps ME, Hoffman EJ, Selin CE, et al. Investigation of [^{18}F]2-fluoro-2-deoxyglucose for the measurement of myocardial glucose metabolism. *J Nucl Med* 1978;19:1311–1319.
13. Hoh CK, Glaspy JA, Choi Y, et al. Quantitative dynamic and whole body PET FDG imaging of breast cancer. *J Nucl Med* 1992;33:828.
14. Folkow B, Neil E. Gastrointestinal and liver circulations. In: *Circulation*. New York: Oxford University Press; 1971:485–493.
15. Hawkins RA, Phelps ME, Huang SC. Effects of temporal sampling glucose metabolic rates, and disruptions of the blood-brain barrier on the FDG model with or without a vascular compartment: studies in human brain tumors with PET. *J Cereb Blood Flow Metab* 1986;6:170–183.
16. Landaw EM, DiStefano JJ. Multiexponential, multicompartmental noncompartmental modeling. II. Data analysis and statistical considerations. *Am J Physiol* 1984;246:R665–677.
17. Akaike H. A new look at the statistical model identification. *IEEE Trans Automat Contr* 1974;AC-19:716–723.
18. Schwarz G. Estimating the dimension of a model. *Ann Stat* 1978;6:461–564.
19. Chen BC, Huang SC, Germano G, et al. Noninvasive quantification of hepatic arterial blood flow with nitrogen-13-ammonia and dynamic positron emission tomography. *J Nucl Med* 1991;32:2219–2208.
20. Niewoehner CB, Nuttall FQ. Relationship of hepatic glucose uptake to intrahepatic glucose concentration in fated rats after glucose load. *Diabetes* 1988;37:1559–1566.
21. Van Schaftingen E, Davies DR. Fructose administration stimulates glucose phosphorylation in the livers of anesthetized rats. *FASEB J* 1991;5:326–330.
22. Lindholm P, Minn H, Leskinen-Kallio S, et al. Influence of the blood glucose concentration on FDG uptake in cancer—a PET study. *J Nucl Med* 1993;34:1–6.

Condensed from
15 Years Ago:

Labeling of Human Platelets with Indium-111-8-Hydroxyquinoline

Ursula Scheffel, Min-Fu Tsan and Patricia A. McIntyre

Division of Nuclear Medicine and Radiation Health Sciences, The Johns Hopkins Medical Institutions, Baltimore, Maryland

The factors influencing the labeling of human platelets in the presence of autologous plasma were evaluated. Labeling efficiency was found to be dependent on: (a) the time and temperature of incubation, (b) the platelet concentration, (c) the concentration of citrate ions (in ACD anticoagulant), and (d) the concentration of 8-hydroxyquinoline in the suspending medium. Contrary to what was expected, unsaturated transferrin was found not to interfere with the transfer of ^{111}In from the [^{111}In]8-hydroxyquinoline complex to the platelets. Based on the findings of this study, a protocol was established by which human platelets can be labeled with ^{111}In in plasma with a labeling efficiency of 55% ± 9% (mean ± 1 s.d.).

J Nucl Med 1979; 20:524-531